

A Review of High-Performance Quantum Dot Lasers on Silicon

Justin C. Norman¹, Member, IEEE, Daehwan Jung, Member, IEEE, Zeyu Zhang², Student Member, IEEE, Yating Wan¹, Songtao Liu, Chen Shang¹, Robert W. Herrick, Senior Member, IEEE, Weng W. Chow, Fellow, IEEE, Arthur C. Gossard, Life Fellow, IEEE, and John E. Bowers³, Fellow, IEEE
(Invited Paper)

Abstract—Laser gain regions using quantum dots have numerous improvements over quantum wells for photonic integration. Their atom-like density of states gives them unique gain properties that can be finely tuned by changing growth conditions. The gain bandwidth can be engineered to be broad or narrow and to emit at a wide range of wavelengths throughout the near infrared. The large energy level separation of the dot states from the surrounding material results in excellent high-temperature performance and gain recovery at sub-picosecond timescales. The fact that the quantum dots are isolated from each other and act independently at inhomogeneously broadened wavelengths results in ultralow linewidth enhancement factors, highly stable broadband mode-locked lasers, single-section mode locking, and the possibility of reduced crosstalk between amplified signals at low signal injection and enhanced four-wave mixing at high signal injection. The high carrier confinement and areal dot density provide reduced sensitivity to crystalline defects allowing for long device lifetimes even when epitaxially grown on silicon at high dislocation densities.

Index Terms—Integrated optoelectronics, photonics, quantum dots, semiconductor lasers.

I. INTRODUCTION

MONOLITHIC photonic integration allows optical systems previously relegated to bulky, bench-scale apparatuses to be developed in compact form factors enabling reduced cost and new applications. In particular, deployable gas and biomolecular sensing systems, lightweight and compact LIDAR components for automobiles, and small footprint, energy efficient interconnects for datacom and telecom

Manuscript received November 1, 2018; revised February 12, 2019; accepted February 14, 2019. Date of publication February 26, 2019; date of current version March 21, 2019. This work was supported in part by the U.S. Department of Energy through the Advanced Research Projects Agency-Energy under Grants DE-AR0000672 and DE-AC04-94AL85000 and in part by the American Institute for Manufacturing Integrated Photonics. (Corresponding author: Justin C. Norman.)

J. C. Norman, C. Shang, and A. C. Gossard are with the Department of Materials, University of California, Santa Barbara, CA 93106 USA (e-mail: jnorman@ucsb.edu).

D. Jung is with the Center for Opto-Electronic Materials and Devices, Korea Institute of Science and Technology, Seoul 02792, South Korea.

Y. Wan, S. Liu, and J. E. Bowers are with the Institute for Energy Efficiency, University of California, Santa Barbara, CA 93106 USA.

Z. Zhang is with the Department of Electrical and Computer Engineering, University of California, Santa Barbara, CA 93106 USA.

R. W. Herrick is with Intel Corporation, Santa Clara, CA 95054 USA.

W. W. Chow is with Sandia National Laboratories, Albuquerque, NM 87185 USA.

Color versions of one or more of the figures in this paper are available online at <http://ieeexplore.ieee.org>.

Digital Object Identifier 10.1109/JQE.2019.2901508

applications are all currently driving development of on-chip photonic integration. In all commercial photonic integrated circuits (PIC) quantum wells (QW) have been utilized as the gain medium of choice. However, there are numerous advantages in terms of performance and economic viability to instead utilizing quantum dots (QD) for many applications.

First proposed in 1982 by Arakawa and Sakaki [1] and demonstrated in 1994 by Kirstaedter *et al.* [2] with Mirin *et al.* [3] showing the first clear evidence of the theorized atom-like density of states, quantum dot lasers have shown numerous performance advantages over QW devices including lower threshold currents [4], higher temperature operation [5], reduced sensitivity to crystalline defects [6], improved stability against optical feedback [7], and ultrafast gain dynamics applicable to semiconductor optical amplifiers (SOA) [8] and mode-locked lasers (MLL) [9]. Each of these advantages comes about from the discrete density of states and inhomogeneously broadened gain spectra unique to the three-dimensional carrier confinement of QDs. Perhaps most notable among these attributes is that their insensitivity to defects allows for epitaxial integration of QD lasers on silicon, and their insensitivity to feedback offers the prospect of eliminating optical isolators in PICs. The former could allow for future laser growth and processing up to the 450 mm scale, or, in the nearer term, for full wafer bonding to be used in 300 mm heterogeneous silicon photonics processes [10].

In the following sections, the basic physical principles of semiconductor QDs will be introduced, and their implications for performance as a gain medium will be explored in the context of recent results. Where possible, results for QD devices grown on silicon will be emphasized to show the robustness of the material system to defects, and potential for more economical production [11].

II. FUNDAMENTALS OF SEMICONDUCTOR QUANTUM DOTS

A. Electronic Density of States

Semiconductor quantum dots can be thought of qualitatively as the textbook case of a particle-in-a-box. The three dimensional quantum confinement provided by band offsets between the narrow gap dot material and surrounding matrix was initially predicted to lead to full discretization of the energy levels into delta-function-like states possessing atom-like degeneracy, in contrast to the step-function-like QW

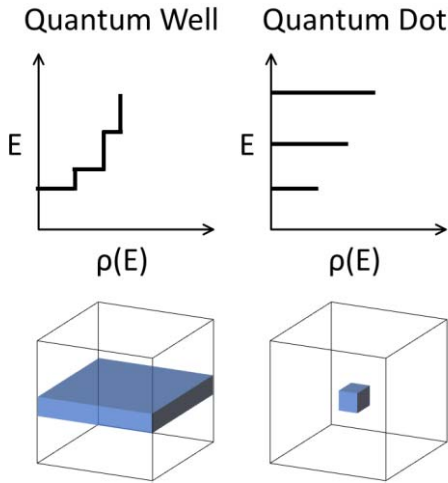


Fig. 1. Schematic illustration of quantum confinement and density of states in quantum wells and dots.

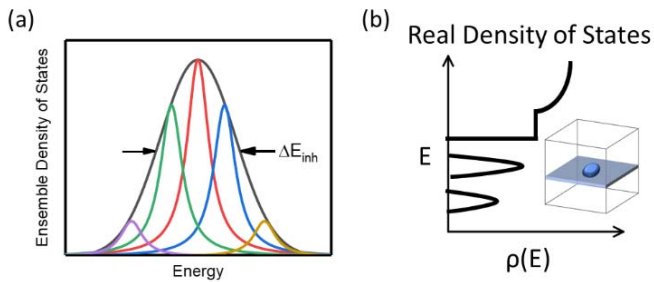


Fig. 2. (a) Schematic illustration of inhomogeneous broadening for a quantum dot state. (b) A realistic schematic of the density of states, $\rho(E)$, of a quantum dot structure including inhomogeneous broadening and the wetting layer.

density of states (DoS), $\rho(E)$ (see Fig. 1). Analogous to the particle-in-a-box, the energy levels of a QD are determined by the size of the dot and height of the potential barrier.

In real semiconductor systems the idealities of the particle-in-a-box picture begin to disappear. The random, self-assembled process of QD formation in crystal growth leads to nonuniformity in the size distribution, strain profile, and compositional fluctuations if non-binary alloys are used for the dots or surrounding matrix. These fluctuations lead to *inhomogeneous broadening*, ΔE_{inh} , of the optical properties of a dot ensemble. The broadening effectively leads to the formation of a quasi-band of states representing the weighted superposition of the discrete states of individual dots, as illustrated in Fig. 2(a). Fortunately, the energy level spacing between principal quantum states can be a few times larger than the inhomogeneous broadening such that the quantized separation can be maintained. An important result of this statistical broadening is that it yields a highly symmetric, Gaussian gain spectrum for the QD states.

The extent of inhomogeneous broadening is dependent on crystal growth conditions and provides additional tunability to the gain spectrum in QD devices, which can be advantageous for broad bandwidth applications such as for optical amplifiers, tunable lasers, and mode-locked lasers. For single-mode lasing with low threshold and high efficiency, a smaller

inhomogeneous broadening is desirable, since off-resonance dots will still capture charge carriers and result in unclamped spontaneous emission. In state-of-the-art QD material, inhomogeneous broadenings, as measured from the photoluminescence spectrum, as low as 24 meV have been realized at room temperature [5].

In further departure from the depiction of Fig. 1, the most well-developed QD material systems form via the Stranski-Krastanov growth mode [12], which yields a thin wetting layer of dot material that acts as a QW connecting all the dots in a layer. A more realistic representation of the DoS of QD material is shown in Fig. 2(b). Atomic force microscopy micrographs of such material are shown in Fig. 3 along with a cross-section transmission electron microscopy image and representative photoluminescence spectrum.

B. Material and Structure

The most well-developed quantum dot materials system is that of In(Ga)As grown on (001) GaAs or InP lattice constant materials. This material system provides the flexibility to obtain luminescence at wavelengths from around 1 μm to 1.8 μm [10] but has been most utilized at the datacom and telecom wavelengths of 1.3 μm and 1.55 μm , respectively. In the less strained InAs/InP system, asymmetric adatom diffusion lengths on the growth surface can lead to lengthening of the QDs in the [011] direction into structures commonly termed “quantum dashes” (QDash). These structures appear to perform as quasi-one dimensional materials with performance characteristics between dots and wells [13].

Depending on the growth conditions and surrounding material chosen, the size, shape, and strain profile of a QD can be changed [14]. These structural changes can have a dramatic effect on the energy level structure of the QDs [15] changing the transition energies, spacing between energy levels, number of confined states, and the ratio of transverse electric (TE) to transverse magnetic (TM) emission [16]. At the ensemble level, the growth conditions will affect the inhomogeneous broadening as discussed previously and the dot density [17], which is typically maximized for laser and amplifier applications to give the maximum gain.

III. QUANTUM DOT DEVICE STRUCTURE

The QD material presented in the following results has been grown using solid source molecular beam epitaxy (MBE). The high degree of tunability in the surface adatom mobility makes MBE an ideal technique for growing optimal QD layers. Additionally, the lower growth temperatures of MBE for Al-containing compounds relative to metalorganic chemical vapor deposition (MOCVD) is beneficial for avoiding harmful intermixing of the QD layers during growth of the top half of the device structure [18], typically a graded-index separate-confinement heterostructure (GRINSCH) composed of 20-50% AlGaAs at a thickness of $\sim 1.5 \mu\text{m}$ for O-band devices and InP or ternary/quaternary arsenide alloys for C-band devices.

The QD devices presented in the following sections are designed for emission around 1300 nm and have the structures

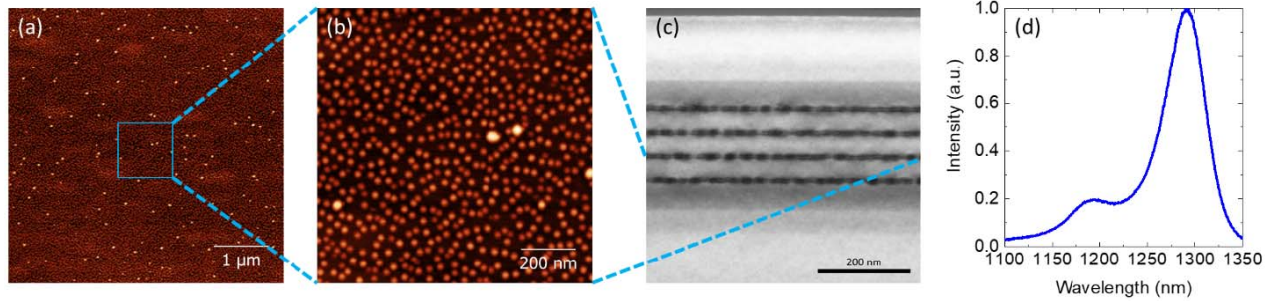


Fig. 3. (a) $5\ \mu\text{m} \times 5\ \mu\text{m}$ atomic force microscopy image of an uncapped quantum dot layer with luminescence around 1300 nm. Larger white spots represent coalesced quantum dots. (b) Zoomed in image from (a). (c) Cross-sectional transmission electron microscope image of four stacked quantum dot layers. (d) Representative photoluminescence spectrum from a single layer of quantum dots.

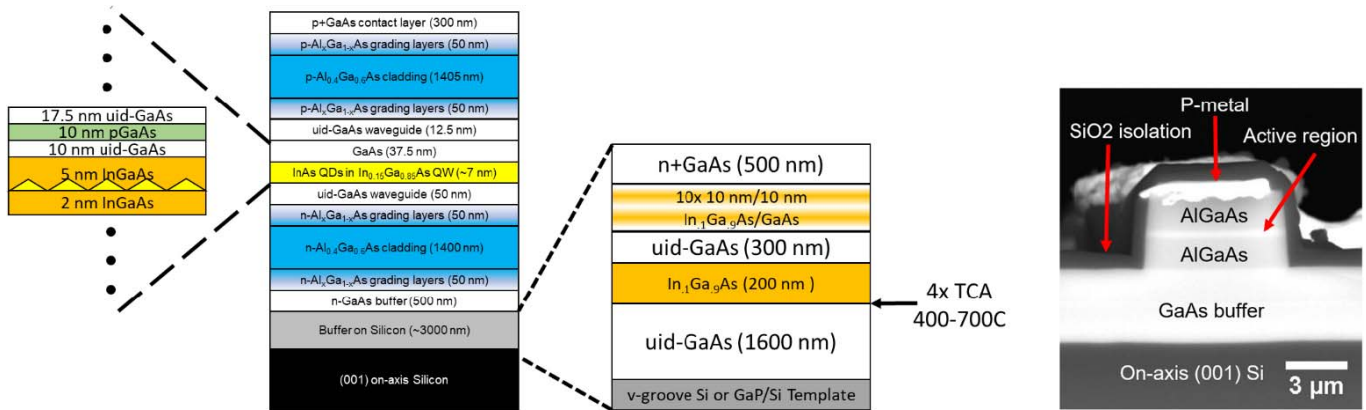


Fig. 4. (Left) Schematic illustration of the epitaxial structure used for lasers and amplifiers including one period of the p-modulation doped active region and the III-V/Si buffer including defect filter layers and thermal cycle annealing (TCA) to reduce dislocation densities (Right) Cross-sectional scanning electron microscope image of a cleaved laser facet.

based on the typical design depicted in Fig. 4. The cladding consists of a $1.4\ \mu\text{m}$ $\text{Al}_{0.4}\text{Ga}_{0.6}\text{As}$ GRINSCH with p-cladding material on top and n-cladding on the bottom. The results shown utilize five to seven periods of InAs quantum dots in 7 nm $\text{In}_{0.15}\text{Ga}_{0.85}\text{As}$ QWs with varied active region doping. The nominal InAs thickness is 2.55 ML, deposited at 500°C and $113\ \text{ML/s}$ with a V/III ratio of 35. The bottom cladding is grown at 580°C while the top cladding is grown at 550°C to minimize interdiffusion in the active region. At these QD growth conditions, dot densities of up to $6.5 \times 10^{10}\ \text{cm}^{-2}$ and photoluminescence (PL) full-width at half maximum (FWHM) as low as 28 meV can be obtained as shown in Fig. 3.

Devices grown on Si contain the buffer structure shown in Fig. 4. For the initial III-V/Si template we have interchangeably used GaP/Si, which is commercially available from NAsP_{III/V}, GmbH, and MOCVD grown GaAs on v-groove patterned Si [19]. Any other template design could be utilized assuming antiphase domains (APD) are eliminated. Demonstrated APD free techniques in addition to those already mentioned include all-MBE growth using AlGaAs nucleation layers on Si [20], MOCVD growth of GaAs on planar silicon [21], and MBE growth of GaAs on homoepitaxial Si or Ge hollow v-groove structures [22].

Devices are processed into laser cavities using inductively coupled plasma dry etching. Sidewall passivation is provided by 30 nm of Al_2O_3 deposited by atomic layer deposition

while electrical isolation is provided by subsequent sputtered deposition of 300 nm SiO_2 . Metal contacts are deposited using electron beam deposition with AuGe/Ni/Au n-contacts and Ti/Pt/Au p-contacts, both top-side contacts.

IV. GAIN IN SEMICONDUCTOR QUANTUM DOTS

A. Independent Emitters

Each individual QD represents an uncorrelated emission source from other spatially separated quantum dots. There is carrier population coupling among quantum dots occurring through the wetting layer QW, which is separated in energy space by a few hundred meV from the dot ground state. The high separation between energy levels means carrier thermalization is relatively suppressed as compared to QW lasers in the InGaAs material system at normal operating temperatures as evidenced by the demonstration of 220°C continuous wave (CW) lasing in a QD laser on GaAs [5], the highest temperature operation of any semiconductor laser, and the demonstration of an athermal optical interposer with error-free data links at 20 Gb/s at 125°C [23]. The net result is that each dot acts independently at its homogeneously broadened energy with the inhomogeneous broadening resulting in a broad energy distribution of independent emitters.

Since each dot can only exhibit stimulated recombination at its energy, the gain it produces is not tied to other dots in

the device with different transition energies. This has positive implications for amplifiers and mode-locked lasers in optical communications. In QW devices, when multiple signals are being amplified simultaneously, cross-gain modulation (XGM) and cross-phase modulation (XPM) can lead to cross-talk between the signals and deteriorate their quality. In a QD amplifier, each wavelength will interact with a different subset of the dot distribution and will not see the spatial and spectral hole burning in the dots at a different wavelength since the charge carriers cannot freely move between dots in the manner that electrons and holes can travel with long diffusion lengths in QWs. The same principles apply for mode-locked lasers where neighboring locked modes will not compete for charge carriers leading to low mode partition noise.

In the high signal regime, QD devices can exhibit enhanced four-wave mixing (FWM) over QWs due to their symmetric gain spectrum, independent emission, and low linewidth enhancement factor [8]. FWM can be useful for applications such as wavelength conversion for signal processing in optical networks. Enhanced FWM in QDs also allows for single-section mode-locked lasers that operate CW with no absorber section [24].

In addition to being independent from each other, the energy ground states of the QD ensemble are also isolated in energy from the wetting layer QW, by 150 meV-200 meV in our 1300 nm material, according to PL. Given that the QD energy levels possess atom-like degeneracy, the carrier density within the dots themselves must be orders of magnitude lower than that of the wetting layer and surrounding material at current injection levels relevant to lasing or amplification. This means that the overall refractive index of the material will be set by a carrier density that is separate from and can be acted on independently from the carrier density responsible for optical gain. Exploiting this property has led to demonstration of 25 Gb/s differential phase shift keying in a QD SOA [25].

B. p-Modulation Doping

To realize most of the previously described theoretical benefits of QD gain media, extra p-type doping must be added to the active layers. For most combinations of III-V materials, the valence band offsets are substantially smaller than those in the conduction band, particularly for the technologically relevant InAs/GaAs and InAs/InP. This leads to energy level spacings in the valence band of ~ 10 meV which is well below kT for room temperature and above applications. As a result, confined holes in QDs can easily thermalize and escape the dots. By adding extra holes through p-type modulation doping (pMD), the effects of thermalization can be compensated thus enhancing population inversion and improving gain in the material [26]–[28]. First principles theory and experimental results have clearly illustrated this property [29] as shown in Fig. 5 which includes a first-principles [30] fit of experimental data obtained via Cassidy's method [31].

Increased pMD does come at a cost, however. The extra holes result in increased nonradiative recombination [32], [33] and optical absorption resulting in higher threshold currents and lower slope efficiencies. These trends are clearly visible

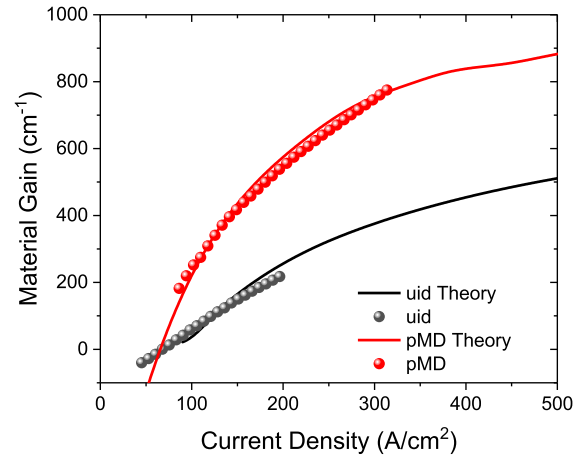


Fig. 5. Theoretical and experimental gain curves for quantum dot lasers with uid and p-modulation doped (pMD) active regions adapted from [29].

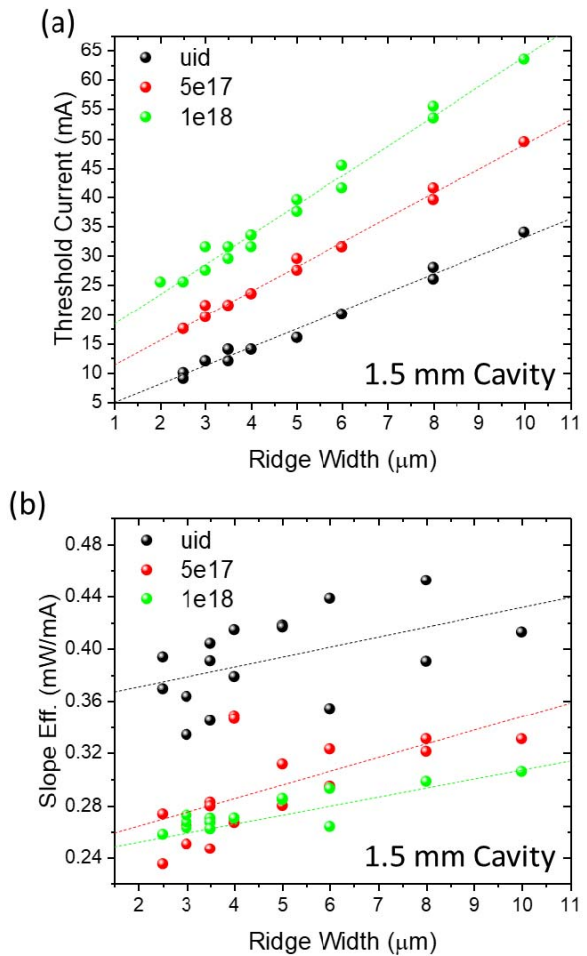


Fig. 6. (a) Threshold current and (b) slope efficiency versus ridge width for a 1.5 mm Fabry-Perot cavity with as-cleaved facets at various p-modulation doping levels in the active region. Adapted from [34].

in Fig. 6 where threshold and slope efficiency are plotted for 1.5 mm Fabry-Perot cavities with five QD layers with varied doping levels including uid, $5 \times 10^{17} \text{ cm}^{-3}$, and $1 \times 10^{18} \text{ cm}^{-3}$ [34]. These doping levels correspond to a ratio of 0, 10, or 20 extra holes per dot, respectively.

C. Ultrafast Gain Recovery

The energy level spacings and decoupling of the gain in QDs from the surrounding carrier reservoir has significant implications for carrier capture processes and gain recovery. Early works regarding QDs had hypothesized that a “phonon bottleneck” would inhibit efficient carrier capture due to the large energy level separation relative to phonon energies [35]. Fortunately, such effects were found to be limited due to efficient Auger processes within QDs allowing for carriers to rapidly relax to the dot ground state on femtosecond time scales [36], [37]. This rapid relaxation leads to sub-picosecond gain recovery times for QD devices—well below the nanosecond recovery times of the well-like wetting layer carrier reservoir [8]. For QWs, the gain and carrier reservoir represent the same carrier population leading to gain recovery times of a few picoseconds to a nanosecond.

Ultrafast gain recovery allows for amplification of high data rate signals and mode-locking with ultrashort pulse widths. Pulse widths less than 400 fs [24] have been demonstrated in QD MLLs, significantly lower than what is achievable in QW-based semiconductor MLLs.

Tunnel injection structures, where an injector QW is placed near the dot active region, have been shown to further improve carrier injection. The QW is designed such that its ground state energy level is one LO phonon above that of a QD state. Then by optimizing the barrier thickness between the dot and well, an efficient tunnel injection process [38] can be achieved which improves gain, high temperature performance [32], [39], and modulation characteristics [40].

D. Linewidth Enhancement Factor

For many photonic applications having a narrow linewidth laser is desirable, and for all integrated applications, stability against undesired reflections from other components, waveguide bends, and imperfections is critical to maintaining laser performance. In both cases, the linewidth enhancement factor, α , is a critical parameter. The linewidth enhancement factor describes the ratio of the change in the real part of the refractive index, n , of the laser medium with carrier density to that of the imaginary part, n_i , with respect to carrier density, N , which can be rewritten in terms of the wavelength, λ , and differential gain, dg/dN as follows.

$$\alpha = -\frac{dn/dN}{dn_i/dN} = -\frac{4\pi}{\lambda} \frac{dn/dN}{dg/dN} \quad (1)$$

The laser linewidth scales as

$$\Delta\nu \propto (1 + \alpha^2) \quad (2)$$

while the critical feedback level, f_{crit} , to induce optical instability scales as

$$f_{crit} \propto \frac{1 + \alpha^2}{\alpha^4}. \quad (3)$$

The functional dependence of α means that lower values can be obtained for materials with high differential gain and a symmetric gain spectrum. Quantum dots are unique in their highly symmetric gain spectrum due to their discrete,

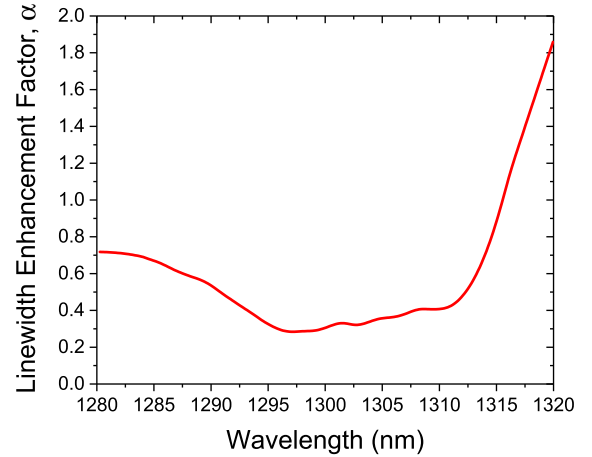


Fig. 7. The linewidth enhancement factor, α , extracted from sub-threshold amplified spontaneous emission is plotted as a function of wavelength for a laser on (001) Si with five p-modulation doped ($5 \times 10^{17} \text{ cm}^{-3}$)

inhomogeneously broadened states which result in a Gaussian profile when superimposed. Furthermore, the decoupling of the gain and carrier reservoir means that changes in the real and imaginary parts of the refractive index are decoupled at higher injection levels leading to a low ratio of $\Delta n/\Delta g$.

Typical values of α for quantum well materials are in the range of 3-5 while we have shown values much less than unity over a broad spectral range in subthreshold measurements (as shown in Fig. 7) and remaining low at higher injection levels [41]. From the scaling relations above, lowering α from 3 to 0.5 should result in a factor of 8 reduction in linewidth and a factor of 162 increase in the critical feedback level. The increased feedback tolerance has been clearly demonstrated in comparisons of our QD material with QW lasers [7] and demonstration of stable operation under feedback levels as high as 90% [42] as reviewed below.

Beyond simply showing near zero α , theoretical calculations and experimental results have shown that for sufficiently low inhomogeneous broadening, negative values can be obtained [30], [43]. Negative values are significant for high power applications where α is sometimes referred to as the antiguiding factor as it relates to spatial hole burning and filamentation. For positive values of α , carrier depletion by the optical mode acts to focus light within the laser cavity leading to further depletion and more focusing in a feedback loop that limits the achievable output power in ridge cavities, particularly for single-mode applications. For negative values of α , the light would be defocused eliminating filamentation.

Due to its impact on gain and differential gain, modulation p-doping strongly affects the linewidth enhancement factor. By varying the p-doping level from 0 to $1 \times 10^{18} \text{ cm}^{-3}$, we have shown subthreshold linewidth enhancement factors from 0.48 to -0.66 as shown in Fig. 8 [44].

V. QUANTUM DOTS FOR EPITAXIAL INTEGRATION ON SILICON

Existing high-performance PICs utilize either an all III-V material platform or silicon with III-V gain integrated through

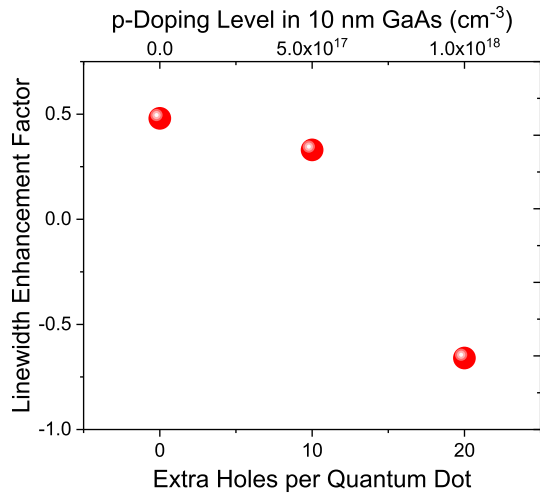


Fig. 8. Sub-threshold linewidth enhancement factor as a function of p-doping level for five-layer quantum dot lasers on silicon. The p-doping level is expressed in terms of the ratio of added holes to the number of quantum dots. Adapted from [44].

co-packaging (hybrid integration) or bonding (heterogeneous integration). The primary advantage of using all III-Vs is that it serves as a native platform for integrating optical gain elements; whereas, silicon provides an economic advantage through the lower cost of wafers and scalability of their larger size and well-developed manufacturing infrastructure, but both hybrid and heterogeneous integration have drawbacks.

The problem inherent to hybrid integration is that it increases packaging complexity and has limited scalability for integrating multiple gain elements. Heterogeneous integration where III-V gain media are bonded onto a processed silicon photonic chip with evanescent coupling of light vertically into silicon waveguides is more promising. Recent advances even show improved performance over monolithic III-V devices [45]. In heterogeneous integration, the challenges arise from the manufacturing complexity of wafer or die bonding and limited scalability due to the reduced size and higher price of III-V substrates relative to Si.

From a manufacturing perspective, the ideal approach is epitaxial integration on silicon [11]. Direct epitaxial growth allows for III-V device production at the Si wafer scale. With a 300 mm or larger III-V/Si platform, the integration method can then take any form [10]. The same techniques used for native substrate III-V devices could be employed with Si serving solely as a low-cost substrate including for full 300 mm wafer-scale bonding. Alternatively, growth could be done on silicon-on-insulator wafers for a silicon photonics approach.

The challenge in epitaxial integration is overcoming the crystalline mismatch that leads to defects in the III-V layers that include dislocations, antiphase domains, and cracks. Antiphase domains can be eliminated through use of miscut Si, or, to maintain CMOS compatibility with on-axis (001) Si, through carefully optimized growth conditions [20], [21], [46], [47] or Si patterning [19], [48]. Cracking can be solved as well through selective area growth if uniform coverage is not required across the full wafer [49] or by allowing the wafer to bow during growth and cooldown. Dislocations

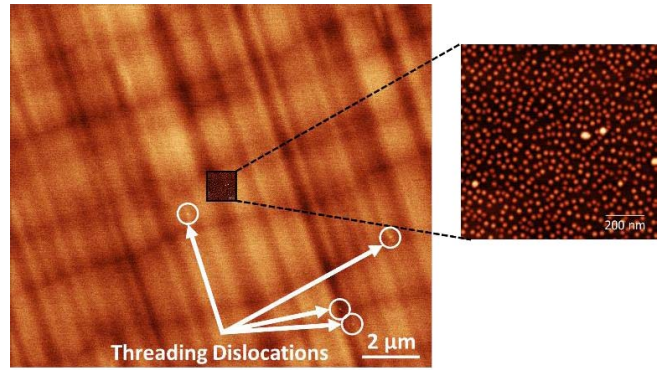


Fig. 9. Plan-view electron channeling contrast image showing four threading dislocations in a GaAs/Si template over a $14.5 \mu\text{m} \times 14.5 \mu\text{m}$ field of view. (inset) Atomic force microscopy image of uncapped quantum dots scaled to the size of the ECCI image to illustrate the high dot:dislocation ratio.

can be managed using strained interlayers, thermal cycling, and selective area growth [50]–[52], but more work remains to be done to match native substrate device performance, particularly regarding device reliability [10], [53]. In the end, though, even one dislocation can result in the failure of a QW device, and dislocation free III-V/Si is likely not achievable at high yield. Fortunately, QDs offer reduced sensitivity to defects.

A. Tolerance to Crystalline Defects

The in-plane carrier confinement provided by QDs inhibits nonradiative recombination at dislocations and other defects. With QD densities as high as $6 \times 10^{10} \text{ cm}^{-2}$ and typical dislocation densities in optimized buffers of $\sim 10^6 \text{ cm}^{-2}$, the likelihood of charge carriers finding a dot before a dislocation is extremely high. The relative densities are illustrated in Fig. 9 which shows an AFM image of QDs drawn to scale with a plan-view electron channeling contrast imaging (ECCI) scan showing dislocations in an optimized GaAs/Si buffer at $7 \times 10^6 \text{ cm}^{-2}$ dislocation density.

The ability for QDs to tolerate residual dislocations has been confirmed in a direct comparison of QD and QW performance on identical III-V/Si templates [6]. At a dislocation density of $7 \times 10^6 \text{ cm}^{-2}$, QD material shows nearly identical room temperature photoluminescence, as shown in Fig. 10. The dot confinement results in higher injection efficiencies which translate into longer device lifetimes by reducing the in-plane carrier diffusion length.

To demonstrate the tolerance of QD gain to dislocations, semiconductor optical amplifier material, with device structure identical to Fig. 4, was grown on a Si substrate with a dislocation density of $7 \times 10^7 \text{ cm}^{-2}$. The active region consisted of seven $5 \times 10^{17} \text{ cm}^{-3}$ pMD QD layers. The SOAs were cleaved from $4 \mu\text{m}$ wide, angled cavities such that the facets had an angle of 8° with a cavity length of 3 mm. No facet coatings were applied. We observed an unsaturated gain factor of 25.4 dB and a saturated input power of 10.9 dBm at a bias of 290 mA. The 3 dB bandwidth of the SOA was 30–40 nm, depending on the bias. The results are shown in Fig. 11 and compare favorably with the native substrate amplifiers in [54].

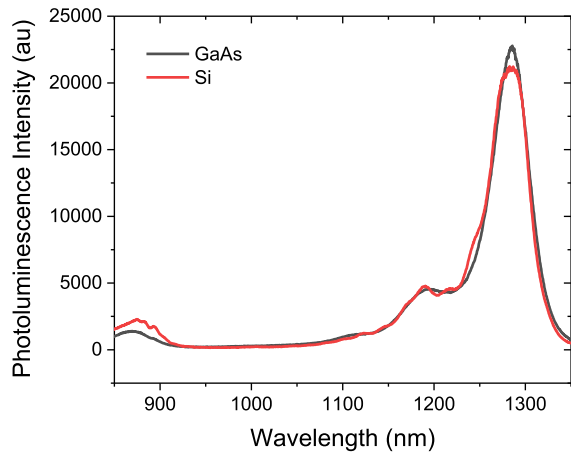


Fig. 10. As-grown photoluminescence spectra for quantum dot lasers on GaAs and Si substrates.

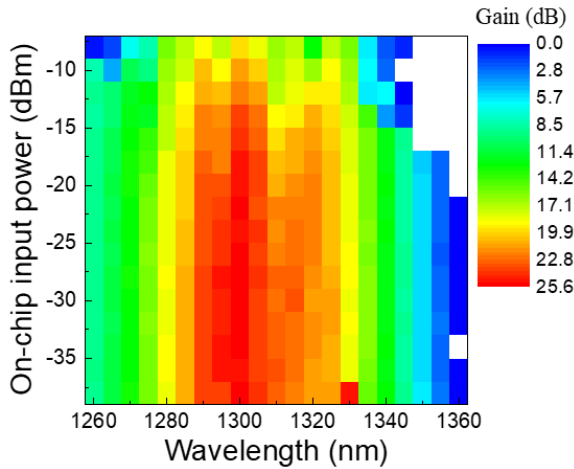


Fig. 11. Gain spectra as a function of on-chip input power for a $4 \mu\text{m} \times 3 \text{mm}$ semiconductor optical amplifier on silicon with seven layers of $5 \times 10^{17} \text{cm}^{-3}$ p-modulation doped quantum dots.

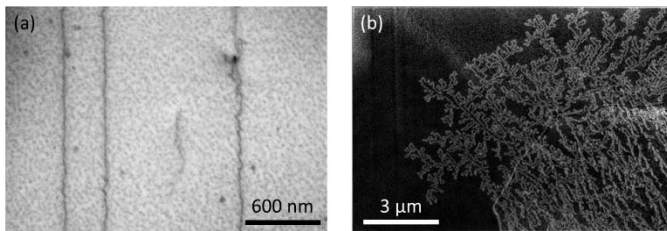


Fig. 12. Plan-view transmission electron microscope image of dislocations in the plane of (a) a quantum dot and (b) a quantum well laser after aging showing the dramatic difference in dislocation climb in the well-based device.

B. Dislocation Climb Inhibition

By reducing the amount of nonradiative recombination at dislocations, the QDs limit the extent of recombination enhanced dislocation climb (REDC) in the material. Fig. 12 shows QD and QW devices containing dislocations aged for a similar amount of time and clear evidence of reduced dislocation climb in the QD material is visible. Only under high magnification can the helical components attributed

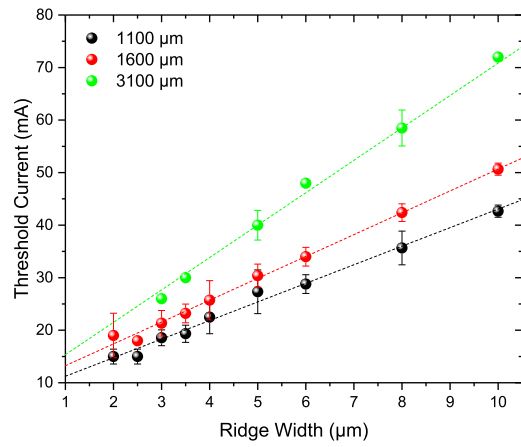


Fig. 13. Threshold current versus ridge width for as-cleaved Fabry-Perot quantum dot lasers at various lengths operating continuous wave at room temperature showing that even for ridges as narrow as $2 \mu\text{m}$, threshold currents still decrease linearly.

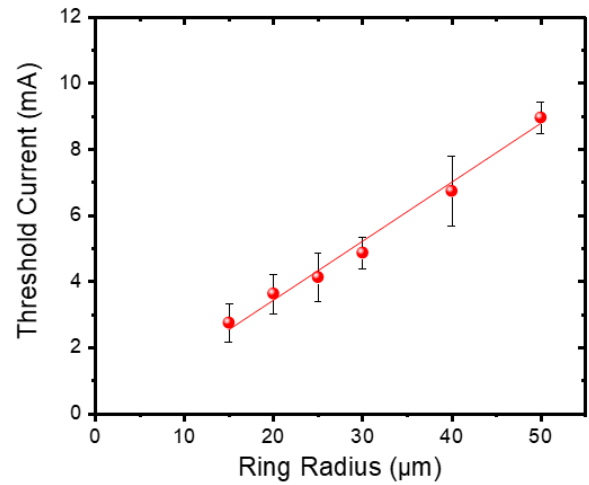


Fig. 14. Threshold current versus ring radius for p-modulation doped microring quantum dot lasers on silicon.

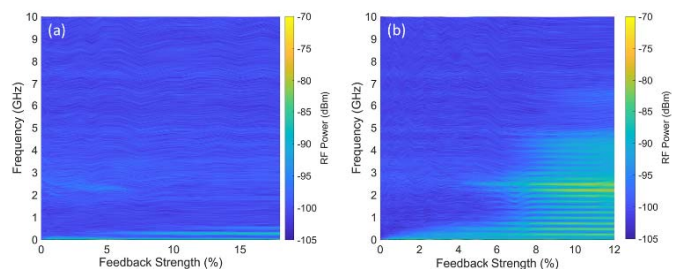


Fig. 15. RF spectra of (a) quantum dot and (b) quantum well devices subjected to varying levels of optical feedback showing highly stable operation from the quantum dot laser up to feedback levels of 18% (adapted from [56]).

to dislocation climb be seen while the QW device shows an extensive network of climb segments.

Through climb inhibition and improved carrier capture, long device lifetimes for QD lasers on Si have been demonstrated. For aging at 35°C , nearly degradation free operation has been observed with extrapolated lifetimes of $> 10,000,000 \text{ h}$

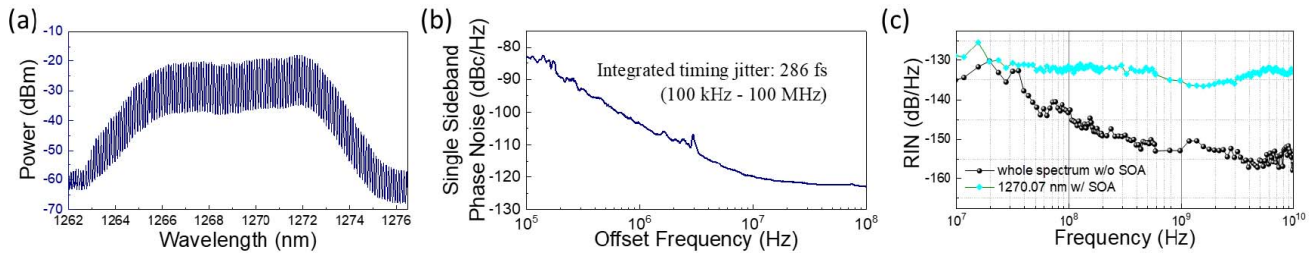


Fig. 16. (a) Optical spectrum from a quantum dot mode-locked laser grown on silicon with (inset) RF electrical spectrum. (b) Single sideband phase noise plot showing record low timing jitter. (c) Relative intensity noise (RIN) spectrum for the entire mode-locked laser spectrum and for an individual comb line after amplification. Adapted from [58].

reported [53]. At 60°C, further improvements are still needed to achieve commercial viability, but recent results utilizing pMD active regions have shown promising extrapolated lifetimes of $\sim 100,000$ h in some devices.

C. Device Miniaturization

For integrated applications, device miniaturization is desirable to increase integration density, but as devices shrink the effects of surfaces, which act as extended planar defects, begin to limit performance. In QD devices, the same properties that reduce sensitivity to dislocations, also reduce their sensitivity to recombination at device sidewalls and other surfaces. In QW lasers the minimum device size is limited by their effective in-plane diffusion length of several microns which causes increasing threshold currents as the laser cavity shrinks in width, but in QD layers, the in-plane diffusion length is ~ 1 μm . Due to limited in-plane diffusion, QD lasers show linearly decreasing thresholds for ridge widths down to 2 μm as depicted in Fig. 13.

Further emphasis of the scalability of QD devices can be seen in the high performance of micron-scale ring resonator cavities. In devices with uid active regions, ultralow thresholds under 1 mA have been demonstrated on Si substrates by scaling to rings with radii of 4 μm [55]. Devices with pMD in the active region analogous to the Fabry-Perot results in Fig. 13 are shown in Fig. 14. The smallest devices, with a radius of 15 μm m, show threshold currents approaching 2 mA.

VI. HIGH LASER STABILITY

A. Stability Against Optical Feedback

As mentioned above, the ultralow values of the linewidth enhancement factor lead to highly stable operation under optical feedback. In a direct comparison of QD lasers on Si with 2×10^8 cm^{-2} dislocation density and >35 meV PL FWHM showed similar relative intensity noise (RIN) at 10 dB higher feedback levels relative to heterogeneous QW devices [7]. After improving the material quality of the QD lasers to 7×10^6 cm^{-2} dislocation density and PL FWHM to ~ 30 meV, the stability against feedback became much more pronounced with stable operation being observed even with 90% of the light reflected back to the cavity (estimated to be 18% feedback after coupling losses) [56].

B. Stable Mode-Locking

The independence of each QD results in low noise mode-locked lasers. Since each inhomogeneously broadened QD acts as an independent emitter, the multiple modes lasing simultaneously with locked phase in a MLL will not compete for gain as they correspond to different subsets of the overall dot distribution. On silicon, heterogeneous devices have been demonstrated with simultaneous error free transmission from 15 channels [57], and epitaxial devices on silicon have shown 4.1 Tb/s transmission using a single MLL grown on Si with a 3dB bandwidth including 58 comb lines (Fig. 16a) that were independently modulated [58]. The latter device showed a record low timing jitter of 286 fs from 100 kHz to 100 MHz (Fig. 16(b)) and low average RIN of -133 dB/Hz for individual comb lines from 10 MHz to 10 GHz (Fig. 16(c)). These performance levels provide further evidence that epitaxial QD lasers on silicon can rival the performance of native substrate devices.

VII. CONCLUSION

In summary, quantum dot lasers enable substantial performance improvements over quantum well devices due to their unique atom-like energy level structure properties that can be finely tuned by changing growth conditions. Their discrete density of states and inhomogeneously broadened gain lead to lasers with low threshold, high continuous wave operating temperature, ultrahigh stability against optical feedback, and ultrafast gain recovery. Each of these concepts has been experimentally demonstrated, and due to the reduced sensitivity of quantum dots to crystalline defects, their advantageous properties are also starting to be shown for epitaxially integrated lasers on silicon, enabling significant improvements in manufacturing scalability.

ACKNOWLEDGMENT

The authors acknowledge valuable discussions with Kunal Mukherjee, Jennifer Selvidge, and Frederic Grillot.

REFERENCES

- [1] Y. Arakawa and H. Sakaki, "Multidimensional quantum well laser and temperature dependence of its threshold current," *Appl. Phys. Lett.*, vol. 40, no. 11, pp. 939–941, 1982.
- [2] N. Kirstaedter *et al.*, "Low threshold, large T_o injection laser emission from (InGa)As quantum dots," *Electron. Lett.*, vol. 30, no. 17, pp. 1416–1417, Aug. 1994.

- [3] R. Mirin, A. Gossard, and J. Bowers, "Room temperature lasing from InGaAs quantum dots," *Electron. Lett.*, vol. 32, no. 18, p. 1732, Aug. 1996.
- [4] D. Bimberg and U. W. Pohl, "Quantum dots: Promises and accomplishments," *Mater. Today*, vol. 14, no. 9, pp. 388–397, 2011.
- [5] T. Kageyama *et al.*, "Extremely high temperature (220 °C) continuous-wave operation of 1300-nm-range quantum-dot lasers," in *Proc. Conf. Lasers Electro-Opt. Eur. 12th Eur. Quantum Electron. Conf. (CLEO EUROPE/EQEC)*, May 2011, p. 1.
- [6] A. Y. Liu, S. Srinivasan, J. Norman, A. C. Gossard, and J. E. Bowers, "Quantum dot lasers for silicon photonics," *Photon. Res.*, vol. 3, no. 5, pp. B1–B9, 2015.
- [7] A. Y. Liu, T. Komljenovic, M. L. Davenport, A. C. Gossard, and J. E. Bowers, "Reflection sensitivity of 1.3 μm quantum dot lasers epitaxially grown on silicon," *Opt. Express*, vol. 25, no. 9, pp. 9535–9543, 2017.
- [8] H. Schmeckebier and D. Bimberg, "Quantum-dot semiconductor optical amplifiers for energy-efficient optical communication," in *Proc. Green Photon. Electron.*, Nov. 2017, pp. 37–74.
- [9] D. Arsenijević and D. Bimberg, "Quantum-dot mode-locked lasers: Sources for tunable optical and electrical pulse combs," in *Proc. Green Photon. Electron.*, Nov. 2017, pp. 75–106.
- [10] J. C. Norman, D. Jung, Y. Wan, and J. E. Bowers, "Perspective: The future of quantum dot photonic integrated circuits," *APL Photon.*, vol. 3, no. 3, Mar. 2018, Art. no. 030901.
- [11] A. Y. Liu and J. Bowers, "Photonic integration with epitaxial III–V on silicon," *IEEE J. Sel. Topics Quantum Electron.*, vol. 24, no. 6, Nov./Dec. 2018.
- [12] R. P. Mirin, J. P. Ibbetson, K. Nishi, A. C. Gossard, and J. E. Bowers, "1.3 μm photoluminescence from InGaAs quantum dots on GaAs," *Appl. Phys. Lett.*, vol. 67, no. 25, pp. 3795–3797, 1995.
- [13] A. J. Zilkie *et al.*, "Carrier dynamics of quantum-dot, quantum-dash, and quantum-well semiconductor optical amplifiers operating at 1.55 μm ," *IEEE J. Quantum Electron.*, vol. 43, no. 11, pp. 982–991, Nov. 2007.
- [14] V. Shchukin, N. N. Ledentsov, and D. Bimberg, *Epitaxy of Nanostructures*. New York, NY, USA: Springer, 2013.
- [15] O. Stier, M. Grundmann, and D. Bimberg, "Electronic and optical properties of strained quantum dots modeled by 8-band k-p theory," *Phys. Rev. B*, vol. 59, nos. 8–15, p. 5688, 1999.
- [16] P. Jayavel *et al.*, "Control of optical polarization anisotropy in edge emitting luminescence of InAs/GaAs self-assembled quantum dots," *Appl. Phys. Lett.*, vol. 84, no. 11, pp. 1820–1822, 2004.
- [17] K. Nishi, K. Takemasa, M. Sugawara, and Y. Arakawa, "Development of quantum dot lasers for data-com and silicon photonics applications," *IEEE J. Sel. Topics Quantum Electron.*, vol. 23, no. 6, Nov./Dec. 2017, Art. no. 1901007.
- [18] A. O. Kosogov *et al.*, "Structural and optical properties of InAs–GaAs quantum dots subjected to high temperature annealing," *Appl. Phys. Lett.*, vol. 69, no. 20, pp. 3072–3074, 1996.
- [19] Q. Li, K. W. Ng, and K. M. Lau, "Growing antiphase-domain-free GaAs thin films out of highly ordered planar nanowire arrays on exact (001) silicon," *Appl. Phys. Lett.*, vol. 106, no. 7, Feb. 2015, Art. no. 072105.
- [20] J. Kwoen, B. Jang, J. Lee, T. Kageyama, K. Watanabe, and Y. Arakawa, "All MBE grown InAs/GaAs quantum dot lasers on on-axis Si (001)," *Opt. Express*, vol. 26, no. 9, pp. 11568–11576, 2018.
- [21] R. Alcotte *et al.*, "Epitaxial growth of antiphase boundary free GaAs layer on 300 mm Si(001) substrate by metalorganic chemical vapour deposition with high mobility," *Apl Mater.*, vol. 4, no. 4, Apr. 2016, Art. no. 046101.
- [22] W.-Q. Wei *et al.*, "InAs QDs on (111)-faceted Si (001) hollow substrates with strong emission at 1300 nm and 1550 nm," *Appl. Phys. Lett.*, vol. 113, no. 5, 2018, Art. no. 053107.
- [23] Y. Urino *et al.*, "First demonstration of Athermal silicon optical interposers with quantum dot lasers operating up to 125 °C," *J. Lightw. Technol.*, vol. 33, no. 6, pp. 1223–1229, Mar. 2015.
- [24] Z. Lu, J. R. Liu, S. Raymond, P. J. Poole, P. J. Barrios, and D. Poitras, "312-fs pulse generation from a passive C-band InAs/InP quantum dot mode-locked laser," *Opt. Express*, vol. 16, no. 14, pp. 10835–10840, 2008.
- [25] A. Zeghuzi *et al.*, "25 Gbit/s differential phase-shift-keying signal generation using directly modulated quantum-dot semiconductor optical amplifiers," *Appl. Phys. Lett.*, vol. 106, no. 21, 2015, Art. no. 213501.
- [26] O. B. Shchekin and D. G. Deppe, "Low-threshold high- T_0 1.3- μm InAs quantum-dot lasers due to p-type modulation doping of the active region," *IEEE Photon. Technol. Lett.*, vol. 14, no. 9, pp. 1231–1233, Sep. 2002.
- [27] O. B. Shchekin, J. Ahn, and D. G. Deppe, "High temperature performance of self-organised quantum dot laser with stacked p-doped active region," *Electron. Lett.*, vol. 38, no. 14, pp. 712–713, Jul. 2002.
- [28] P. M. Smowton, I. C. Sandall, H. Liu, and M. Hopkinson, "Gain in p-doped quantum dot lasers," *J. Appl. Phys.*, vol. 101, no. 1, 2007, Art. no. 013107.
- [29] Z. Zhang, D. Jung, J. C. Norman, P. Patel, W. W. Chow, and J. E. Bowers, "Effects of modulation p-doping in InAs quantum dot lasers on silicon," *Appl. Phys. Lett.*, vol. 113, no. 6, 2018, Art. no. 061105.
- [30] W. W. Chow and F. Jahnke, "On the physics of semiconductor quantum dots for applications in lasers and quantum optics," *Progr. Quantum Electron.*, vol. 37, no. 3, pp. 109–184, 2013.
- [31] D. T. Cassidy, "Technique for measurement of the gain spectra of semiconductor diode lasers," *J. Appl. Phys.*, vol. 56, no. 11, pp. 3096–3099, 1984.
- [32] S. Fathpour *et al.*, "The role of Auger recombination in the temperature-dependent output characteristics (T_∞) of p-doped 1.3 μm quantum dot lasers," *Appl. Phys. Lett.*, vol. 85, no. 22, pp. 5164–5166, 2004.
- [33] P. M. Smowton, A. George, I. C. Sandall, M. Hopkinson, and H.-Y. Liu, "Origin of temperature-dependent threshold current in p-doped and Undoped In(Ga)As quantum dot lasers," *IEEE J. Sel. Topics Quantum Electron.*, vol. 14, no. 4, pp. 1162–1170, Jul./Aug. 2008.
- [34] J. C. Norman *et al.*, "High performance quantum dot lasers epitaxially integrated on Si," in *Proc. 16th Quantum Commun. Quantum Imag.*, vol. 10771, Art. no. 107710D.
- [35] M. Sugawara, K. Mukai, and H. Shoji, "Effect of phonon bottleneck on quantum-dot laser performance," *Appl. Phys. Lett.*, vol. 71, no. 19, pp. 2791–2793, 1997.
- [36] T. W. Berg, S. Bischoff, I. Magnusdottir, and J. Mork, "Ultrafast gain recovery and modulation limitations in self-assembled quantum-dot devices," *IEEE Photon. Technol. Lett.*, vol. 13, no. 6, pp. 541–543, Jun. 2001.
- [37] K. Kim, J. Urayama, T. B. Norris, J. Singh, J. Phillips, and P. Bhattacharya, "Gain dynamics and ultrafast spectral hole burning in In(Ga)As self-organized quantum dots," *Appl. Phys. Lett.*, vol. 81, no. 4, pp. 670–672, 2002.
- [38] P. Bhattacharya *et al.*, "Carrier dynamics and high-speed modulation properties of tunnel injection InGaAs-GaAs quantum-dot lasers," *IEEE J. Quantum Electron.*, vol. 39, no. 8, pp. 952–962, Aug. 2003.
- [39] Z. Mi and P. Bhattacharya, "DC and dynamic characteristics of P-doped and tunnel injection 1.65- μm InAs quantum-dash lasers grown on InP (001)," *IEEE J. Quantum Electron.*, vol. 42, no. 12, pp. 1224–1232, Nov. 2006.
- [40] Z. Mi, P. Bhattacharya, and S. Fathpour, "High-speed 1.3 μm tunnel injection quantum-dot lasers," *Appl. Phys. Lett.*, vol. 86, no. 15, 2005, Art. no. 153109.
- [41] J. Duan *et al.*, "Semiconductor quantum dot lasers epitaxially grown on silicon with low linewidth enhancement factor," *Appl. Phys. Lett.*, vol. 112, no. 25, 2018, Art. no. 251111.
- [42] H. Huang *et al.*, "Analysis of the optical feedback dynamics in InAs/GaAs quantum dot lasers directly grown on silicon," *J. Opt. Soc. Amer. B*, vol. 35, no. 11, pp. 2780–2787, 2018.
- [43] P. M. Smowton, E. J. Pearce, H. Schneider, W. W. Chow, and M. Hopkinson, "Filamentation and linewidth enhancement factor in InGaAs quantum dot lasers," *Appl. Phys. Lett.*, vol. 81, no. 17, pp. 3251–3253, 2002.
- [44] Z. Zhang, D. Jung, J. C. Norman, P. Patel, W. W. Chow, and J. E. Bowers, "Across zero continuously tunable linewidth enhancement factor in 1.3 μm InAs quantum dot lasers on silicon," in *Proc. 26th Int. Semicond. Laser Conf.*, Santa Fe, NM, USA, 2018.
- [45] T. Komljenovic, D. Huang, P. Pintus, M. A. Tran, M. L. Davenport, and J. E. Bowers, "Photonic integrated circuits using heterogeneous integration on silicon," *Proc. IEEE*, vol. 106, no. 12, pp. 2246–2257, Dec. 2018.
- [46] S. Chen *et al.*, "Electrically pumped continuous-wave 1.3 μm InAs/GaAs quantum dot lasers monolithically grown on on-axis Si (001) substrates," *Opt. Express*, vol. 25, no. 5, pp. 4632–4639, 2017.
- [47] B. Kunert, I. Németh, S. Reinhard, K. Volz, and W. Stolz, "Si (001) surface preparation for the antiphase domain free heteroepitaxial growth of GaP on Si substrate," *Thin Solid Films*, vol. 517, no. 1, pp. 140–143, 2008.
- [48] M. Paladugu *et al.*, "Site selective integration of III–V materials on Si for nanoscale logic and photonic devices," *Crystal Growth Des.*, vol. 12, no. 10, pp. 4696–4702, 2012.

- [49] H. Huang *et al.*, "Crack-free GaAs epitaxy on Si by using midpatterned growth: Application to Si-based wavelength-selective photodetector," *J. Appl. Phys.*, vol. 104, no. 11, 2008, Art. no. 113114.
- [50] M. Tang *et al.*, "Optimizations of defect filter layers for 1.3- μm InAs/GaAs Quantum-Dot Lasers Monolithically grown on Si substrates," *IEEE J. Sel. Topics Quantum Electron.*, vol. 22, no. 6, Nov./Dec. 2016.
- [51] D. Jung, P. G. Callahan, B. Shin, K. Mukherjee, A. C. Gossard, and J. E. Bowers, "Low threading dislocation density GaAs growth on on-axis GaP/Si (001)," *J. Appl. Phys.*, vol. 122, no. 22, p. 225703, 2017.
- [52] E. Fitzgerald and N. Chand, "Epitaxial necking in GaAs grown on pre-patterned Si substrates," *J. Electron. Mater.*, vol. 20, no. 7, pp. 839–853, 1991.
- [53] D. Jung *et al.*, "Impact of threading dislocation density on the lifetime of InAs quantum dot lasers on Si," *Appl. Phys. Lett.*, vol. 112, no. 15, 2018, Art. no. 153507.
- [54] M. Kuntz, G. Fiol, M. Laemmlin, C. Meuer, and D. Bimberg, "High-speed mode-locked quantum-dot lasers and optical amplifiers," *Proc. IEEE*, vol. 95, no. 9, pp. 1767–1778, Sep. 2007.
- [55] Y. Wan *et al.*, "1.3 μm submilliwatt threshold quantum dot micro-lasers on Si," *Optica*, vol. 4, no. 8, pp. 940–944, 2017.
- [56] J. Duan *et al.*, "1.3- μm reflection insensitive InAs/GaAs quantum dot lasers directly grown on silicon," *IEEE Photon. Technol. Lett.*, vol. 31, no. 5, pp. 345–348, Mar. 1, 2019.
- [57] G. Kurczveil, C. Zhang, A. Descos, D. Liang, M. Fiorentino, and R. G. Beausoleil, "On-chip hybrid silicon quantum dot comb laser with 14 error-free channels," in *Proc. IEEE Int. Semicond. Laser Conf. (ISLC)*, Santa Fe, NM, USA, Sep. 2018, pp. 1–2.
- [58] S. Liu *et al.*, "High-channel-count 20 GHz passively mode-locked quantum dot laser directly grown on Si with 4.1 Tbit/s transmission capacity," *Optica*, vol. 6, no. 2, pp. 128–134, 2018.



Zeyu Zhang (S'17) received the B.S. degree in electrical engineering from Clemson University, SC, USA, in 2015. He is currently pursuing the Ph.D. degree with the University of California, Santa Barbara, CA, USA.

His research interests include the characterization and modeling of quantum dot laser epitaxially grown on silicon as well as passive-active integration of photonic devices with quantum dot active region on monolithic III-V on silicon platform.



Yating Wan received the Ph.D. degree from the Department of Electrical and Computer Engineering, The Hong Kong University of Science and Technology, in 2017. In 2017, she joined Prof. J. E. Bowers's Group, University of California, Santa Barbara, as a Post-Doctoral Research Associate. Her research interests include microcavity quantum dot optoelectronics and silicon photonics. She was a recipient of the Ph.D. Research Excellence Award during 2016–2017.



Justin C. Norman (S'14–M'18) received the B.S. degree in chemical engineering and physics from the University of Arkansas at Fayetteville, Fayetteville, AR, USA, in 2013, and the Ph.D. degree in materials from the University of California, Santa Barbara, with a focus on the epitaxial growth of quantum dot lasers for silicon photonics.

He is currently a Post-Doctoral Researcher with the Institute for Energy Efficiency, University of California. He focuses on the heteroepitaxy of III-V materials on Si for photonic integration. His research

interests are in the growth of InAs quantum dots via molecular beam epitaxy for applications in photonics and quantum electrodynamics. He was a recipient of the National Science Foundation Graduate Research Fellowship and the Frenkel Foundation Fellowship.



Songtao Liu received the B.E. degree (Hons.) in electronic information science and technology from Henan University, Kaifeng, China, in 2012, and the Ph.D. degree in microelectronics and solid state electronics from the University of Chinese Academy of Sciences, Beijing, China, 2017.

His Ph.D. dissertation was on the monolithically integrated InP-based mode-locked lasers. He is currently a Post-Doctoral Researcher with the University of California, Santa Barbara, CA, USA. His research interests are in the field of photonic inte-

grated circuits, with an emphasis on monolithically integrated mode-locked lasers and tunable lasers both on InP and silicon platforms.



Daehwan Jung (M'16) received the Ph.D. degree in electrical engineering from Yale University in 2016. He was a Post-Doctoral Researcher with the University of California, Santa Barbara. He is currently with the Center for Opto-Electronic Materials and Devices, Korea Institute of Science and Technology, Seoul, South Korea. His current research project is to develop highly reliable, high-performance quantum dot lasers epitaxially grown on silicon for communication applications. His primary research interest is to study novel III-V materials growth for high-performance optoelectronic and photonic devices.



Chen Shang received the B.S. degree in material science and engineering from Purdue University, IN, USA, in 2016. He is currently pursuing the Ph.D. degree in materials with the University of California, Santa Barbara, CA, USA.

His research interests are InAs quantum dots on InP lattice constant for telecom application and low defect density III-V buffer structure grown on Si via molecular beam epitaxy. He was a recipient of the Peter J. Frenkel Foundation Fellowship.



Robert W. Herrick (S'81–M'87–SM'05) received the M.S.E.E. degree from the University of Illinois in 1987. His career started at McDonnell Douglas, focusing on the early optoelectronic integrated circuit and high-power laser research and development, where he involved in device modeling, mask design, and process development. After gaining an interest in reliability physics from the late Dr. R. G. Waters, he went to UCSB and did the first studies of VCSEL degradation for his Ph.D. dissertation with Prof. L. Coldren and Prof. P. Petroff. In the past

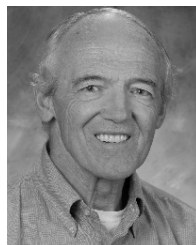
20 years, he has specialized in semiconductor laser reliability and failure analysis. Since 2013, he has been with Intel, where he is currently responsible for laser reliability in the Silicon Photonic Product Division. He has been a Laser Reliability Engineer for many of the large fiber-optics companies in Silicon Valley, including HP/Agilent, Emcore, Finisar, and JDSU/Lumentum. He has authored or co-authored many of the most cited papers and invited book review chapters on the subject.



Weng W. Chow (F'09) received the Ph.D. degree in physics from The University of Arizona, with a focus on the research involving fluctuation phenomena in quantum optics.

He is currently a Member of the Technical Staff with Sandia National Laboratories, where his primary research involves applying microscopic theory to semiconductor laser development. Some of this work is described in two texts, *Semiconductor-Laser Physics* and *Semiconductor-Laser Fundamentals: Physics of the Gain Materials*. He is also an

Honorary Professor of physics with Cardiff University and a fellow with the Institute for Quantum Science and Engineering, Texas A&M University. He is a fellow of OSA. He was a recipient of the Department of Energy, Basic Energy Science/Material Science Award, the J. J. Thompson Premium, the LEOS Distinguished Lecturer Award, the Alexander von Humboldt Senior Scientist Award, and the IEEE Photonics Society Quantum Electronics Award.



Arthur C. Gossard (SM'88–F'01–LF'12) was born in Ottawa, IL, USA, in 1935. He received the B.A. degree (*summa cum laude*) in physics from Harvard University, Cambridge, MA, USA, in 1956, and the Ph.D. degree in physics from the University of California at Berkeley, Berkeley, CA, USA, in 1960.

He was a Member of Technical Staff with AT&T Bell Telephone Laboratories from 1960 to 1987. Since 1987, he has been with the University of California at Santa Barbara, Santa Barbara, CA, USA, where he became a Professor in 1988. He discovered the first nuclear magnetic resonance in ferromagnets. He also grew the first alternate monolayer superlattices and created the first high mobility modulation doped semiconductors. He co-discovered fractional quantization of the quantum Hall effect and the quantum confined Stark effect. His current research interests center on molecular beam epitaxial crystal growth and on the creation and application of artificially structured quantum materials.

Dr. Gossard is a member of the American Physical Society, the Materials Research Society, the National Academy of Sciences, and the National Academy of Engineering.



John E. Bowers (F') received the M.S. and Ph.D. degrees from Stanford University. He was with AT&T Bell Laboratories. He is currently the Director of the Institute for Energy Efficiency, University of California, Santa Barbara. He is also a Professor with the Department of Electrical and Computer Engineering, University of California, and the Department of Materials, University of California. His research interests are primarily concerned with silicon photonics, optoelectronic devices, optical switching and transparent optical networks, and quantum dot lasers. He is a member of the National Academy of Engineering and the National Academy of Inventors. He is a fellow of OSA and the American Physical Society. He was a recipient of the IEEE Photonics Award, the OSA/IEEE Tyndall Award, the IEEE LEOS William Streifer Award, and the South Coast Business and Technology Entrepreneur of the Year Award.